

Numerical modelling of cold helium safety discharges from the cryogenic distribution line

Jonathan Persson



LUND
UNIVERSITY

Department of Automatic Control

MSc Thesis
TFRT-6117
ISSN 0280-5316

Department of Automatic Control
Lund University
Box 118
SE-221 00 LUND
Sweden

© 2020 by Jonathan Persson. All rights reserved.
Printed in Sweden by Tryckeriet i E-huset
Lund 2020

Contents

1. Introduction	9
1.1 European Spallation Source (ESS)	9
1.2 Cryogenic setup at ESS	9
1.3 Project aim	11
2. Theory	13
2.1 Fluid dynamics	13
2.2 Gas Dynamics	14
3. Methods	19
3.1 Method overview	19
3.2 Problem description	20
3.3 Choice of software	22
3.4 Pre-processing	23
3.5 Solver	27
3.6 Post-processing	27
4. Results	28
4.1 Benchmarking	28
4.2 ESS CDL ventilation (HVL)	29
5. Discussion	43
6. Conclusion	44
6.1 Recommendations / Future work	44
7. Appendices	45
7.1 Appendix - Model assumptions	45
7.2 Appendix 3 - Code	46
Bibliography	49

Abstract

The European Spallation Source, ESS, is a project currently with 17 Partner Countries, and with Sweden and Denmark as host nations. The ESS main facility is being constructed in Lund, to ultimately become the world's most powerful neutron source, providing around 30 times brighter neutron beams than any earlier facility.

The Linear Accelerator, Linac, at the heart of ESS is fundamentally powered by superconducting cavities that require extremely low temperatures to operate, namely 2K (-271 °C). The cooling/cryogenic fluid, helium, is supplied to the cavities through a complex cryogenic distribution system (CDS). At abnormal failure modes, to protect against unwanted over-pressurisation, this system needs to be vented through pressure safety valves. To avoid helium discharges into the tunnel the safety valves will discharge cold helium into a vent line, which transfer the helium into the external environment. Usually the most critical failure mode is a loss of insulation vacuum, which exposes the CDS to a sudden rise of heat loads.

This thesis investigates the most critical phenomena for the non-insulated vent line flows. Due to a lack of simple engineering descriptions of these unsteady flows, a set of complex numerical models will support a proper vent line sizing proposal. A commercial numerical software, ANSYS Fluent, is used and compared with simpler solution methods for differential equations derived from Fanno and Rayleigh flow theories.

Acknowledgements

I wish to show my gratitude to everyone that have helped and assisted in the work of this thesis.

At ESS, thank you Prof. John Weisend II and Dr. Jarosław Fydrych for all the guidance in understanding the physical processes involved.

At Lund University, Department of Automatic Control, thank you Prof. Rolf Johansson, for help with planning, conducting and documenting the thesis work.

Also, I would like to thank Prof. Johan Revstedt, for help with numerical modelling aspects of fluid mechanical systems.

Abbreviations

CDL - Cryogenic Distribution Line

CDS - Cryogenic Distribution System

CFD - Computational Fluid Dynamics

CTL - Cryogenic Transfer Line

DN - Diamètre Nominal (fr.). Nominal diameter, ISO standard for the pipe diameter that identifies the approximate inner diameter with a non-dimensional number. Pipes having identical nominal diameters can be easily connected or interchanged with each other [*Pipework components — Definition and selection of DN (nominal size)* 1995].

ESS - European Spallation Source

FEM - Finite Element Method

GHe - gaseous helium

He - Helium

HVL - Helium Vent Line (model), the abbreviation for the main numerical simulation setup in this thesis

Linac - Linear accelerator

LHe - liquid helium

ODH - Oxygen deficiency hazard

pn - Pressure Nominal (fr.). Nominal pressure, ISO standard for the maximum internal pressure that the pipe and its joints are capable of withstanding, expressed in bars [*Pipe components — Definition of nominal pressure* 1983].

RANS - Reynolds-averaged Navier–Stokes

RF - radiofrequency

VLP - vacuum low pressure

Symbols

T - temperature

Symbols subscript:

$()_0$ - Zero, indicating total/stagnation property, e.g., stagnation pressure p_0

He - Helium

N_2 - Nitrogen

ss - stainless steel

1

Introduction

1.1 European Spallation Source (ESS)

The European Spallation Source, currently under construction in Lund, Sweden, is a neutron science facility for academic and industrial research set to answer scientific questions using neutron beams [Peggs and (Ed.), 2013, pg.1].

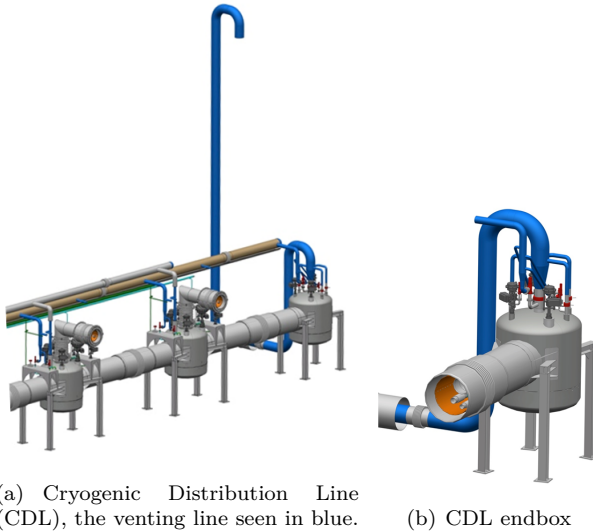
In the ESS, protons are accelerated in a linear accelerator (linac) to hit a wolfram target. At impact with the target, neutrons are splintered away by the high-energy incoming protons. The impact process at which an outgoing neutron stream is produced is called spallation [Weisend II et al., 2014].

The facility is planned to deliver its first neutrons to the initial set of instruments in 2019, and to fulfill the final specifications in 2025. The final setup describes an accelerator operating at 5 MW proton power. A large set of neutron scattering instruments, 22, will be used for analysis. The ESS will ultimately be serving a large user community to generate top-class science [Peggs and (Ed.), 2013, pg.1]. ESS will offer to produce a neutron beam of unparalleled intensity and of flexible pulse time, up to 3 *ms* [Eriksson, 2008].

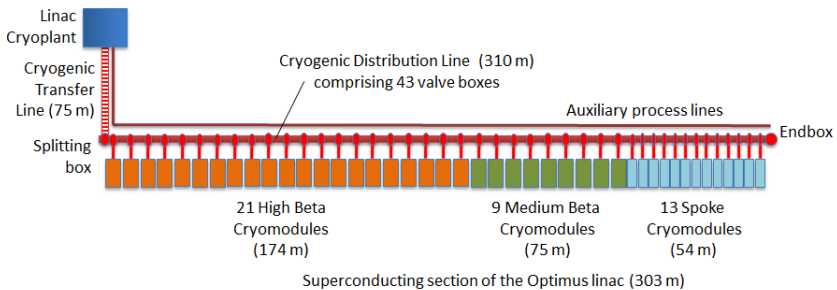
The centerpiece of ESS, the 2.5 GeV proton linear accelerator (linac), uses superconducting radiofrequency (RF) cavities operating at cryogenic temperatures, 2K [Weisend II et al., 2014, pg.633].

1.2 Cryogenic setup at ESS

The cryogenic system consists of: the linac cryoplant that provides cooling for cryomodules, the test and instrumentation cryoplant that provides cooling for test stands and liquid helium for instruments, the target cryoplant that provides 16K helium cooling for the target hydrogen moderators, and the distribution system that connects the linac cryoplant to cryomodules [Peggs and (Ed.), 2013]. This project deals exclusively with the latter, the distribution system.



The ESS cryogenic system contains two separate parts; one serving the target section of the facility and the other providing cryogenic services to accelerator cryomodules, the instruments and experiments section, and for the test stand [Peggs and (Ed.), 2013, pg.450]. In the latter system part we find the the Linac Cryogenic System, consisting of a cryoplant, a transfer line and a set of cryomodules connected to the linac. The pipe connecting the transfer line (CTL) to the individual cryomodules is the cryogenic distribution line (CDL), which is the main system part of interest in this project.



When assessing the risks for a specified part of the cryogenic system, a risk analysis is performed, and the different risk scenarios are estimated on the basis of prior knowledge. In the case at hand, for the CDL, the main risk

is predicted to be the event of a sudden loss of the insulating vacuum surrounding the CDL pipe. The main concerns involving a loss of the insulating vacuum and the subsequent remarkably rapid heat transfer to the CDL, are twofold; the protection of equipment within the CDL and its interconnected parts, but foremost the oxygen deficiency hazard (ODH) to which any personnel working in the tunnel is subjected. The helium within the CDL will very quickly be heated and try to expand, the pressure will rise as an effect and the CDL pipe (of standard pn6, i.e. tolerating an absolute pressure of 6 bar) will either have to be relieved or rupture incalculably.

1.3 Project aim

The aim of this project was to investigate the possibilities of venting the CDL into the atmosphere. This is a measure deemed reasonable as a response to some dangerous failure modes. If deemed possible and even optimal, the project objective was to evaluate a suggested pipe sizing for such a venting function. Candidates for suggested sizing were tested, by performing a set of numerical simulations. These simulations aimed to resemble the real venting situation as closely as possible and include the physical processes of highest relevance. The simulations were then benchmarked with a semi-numerical approach based on Fanno and Rayleigh flows from the theory of gas dynamics, based on a simpler model taking less processes into account. The semi-numerical model was tuned to better approximate the simulations.

Problem formulation

Due to the lack of simple engineering descriptions of these flows the proper sizing of the vent line shall be supported by a complex numerical modeling, which takes into account all significant phenomena occurring during the safety discharges.

Scope of the work:

1. Study of all the processes occurring during the analyzed safety discharges (unsteady flow, compressible flow, mixing of fluids in different thermodynamic states, diffusion, back pressure effect, cryogenic heat transfer, frosting, air condensation, etc.),
2. Investigation into the importance of the listed processes,
3. Mathematical description of the chosen processes,
4. Development of a numerical code,
5. Validation and/or benchmarking of the code,

6. Numerical modeling of the safety discharges,
7. Recommendation on the vent line size.

Assumptions & simplifications The numerical results produced in this thesis do not assume the form of an answer to a well-defined problem (in the textbook sense); rather, the results are the product of a larger set of simulations and will work as a decision basis for future design. The surrounding environment and circumstances are not well-defined and the same can be said about the set of failure modes. By providing a carefully selected set of simulations, a highly probable course of events is possible to evaluate.

The bulk of the work conducted was aimed at creating a numerical model of high accuracy and quality, supported by the simpler semi-numerical approach and validated by the closest experimental results at hand. The main parameter of interest is the mass flow rate. For transient simulations, the peak mass flow rate was the one of focus [Fydrych, 2014].

2

Theory

2.1 Fluid dynamics

Classical Fluid Dynamics

The compressible Euler and Navier-Stokes equations represent the most sophisticated models of single-phase flows of single-component Newtonian fluids. As such, they allow the analysis of complex inviscid and viscous flow phenomena including rotational flows caused by curved shock waves or viscous/inviscid interactions leading to flow separation. As a counterpart, the numerical techniques required to solve these equations are also the most sophisticated and the numerical effort needed to obtain them is also the greatest [Anderson Jr. et al., 2009, pg. 183].

Governing Equations Fundamentally CFD is based on a set of governing equations of fluid dynamics, that represent mathematical statements of the conservation laws of physics; the conservation of mass, momentum and energy. Commonly, the three are referred to as the continuity equation, Newton's second law and the first law of thermodynamics.

Ordinary formulation For all flows, ANSYS Fluent solves conservation equations for mass and momentum. For flows involving heat transfer or compressibility, an additional equation for energy conservation is solved. Additional transport equations are solved when the flow is turbulent [ANSYS CFX-Solver Theory Guide 2013, pg. 2].

$$\frac{\partial \rho}{\partial t} + \nabla \cdot (\rho \vec{v}) = S_m \quad (2.1)$$

$$\frac{\partial}{\partial t}(\rho \vec{v}) + \nabla \cdot (\rho \vec{v} \vec{v}) = -\nabla p + \nabla \cdot (\bar{\tau}) + \rho \vec{g} + \vec{F} \quad (2.2)$$

$$\bar{\tau} = \mu \left[(\nabla \vec{v} + \nabla \vec{v}^T) - \frac{2}{3} \nabla \cdot \vec{v} I \right] \quad (2.3)$$

Axisymmetric 2D simulation

$$\frac{\partial \rho}{\partial t} + \frac{\partial}{\partial x}(\rho v_x) + \frac{\partial}{\partial r}(\rho v_r) + \frac{\rho v_r}{r} = S_m \quad (2.4)$$

$$\begin{aligned} & \frac{\partial}{\partial t}(\rho v_x) + \frac{1}{r} \frac{\partial}{\partial x}(r \rho v_x^2) + \frac{1}{r} \frac{\partial}{\partial r}(r \rho v_r v_x) \\ &= -\frac{\partial p}{\partial x} + \frac{1}{r} \frac{\partial}{\partial x} \left[r \mu \left(2 \frac{\partial v_x}{\partial x} - \frac{2}{3} (\nabla \cdot \vec{v}) \right) \right] + \frac{1}{r} \frac{\partial}{\partial r} \left[r \mu \left(\frac{\partial v_x}{\partial r} + \frac{\partial v_r}{\partial x} \right) \right] + F_x \end{aligned} \quad (2.5)$$

$$\begin{aligned} & \frac{\partial}{\partial t}(\rho v_r) + \frac{1}{r} \frac{\partial}{\partial x}(r \rho v_x v_r) + \frac{1}{r} \frac{\partial}{\partial r}(r \rho v_r^2) \\ &= -\frac{\partial p}{\partial r} + \frac{1}{r} \frac{\partial}{\partial x} \left[r \mu \left(\frac{\partial v_r}{\partial x} + \frac{\partial v_x}{\partial r} \right) \right] \\ & \quad + \frac{1}{r} \frac{\partial}{\partial r} \left[r \mu \left(2 \frac{\partial v_r}{\partial r} - \frac{2}{3} (\nabla \cdot \vec{v}) \right) \right] - 2\mu \frac{v_r}{r^2} + \frac{2}{3} \frac{\mu}{r} (\nabla \cdot \vec{v}) + \rho \frac{v_z^2}{r} + F_r \end{aligned} \quad (2.6)$$

$$\nabla \cdot \vec{v} = \frac{\partial v_x}{\partial x} + \frac{\partial v_r}{\partial r} + \frac{v_r}{r} \quad (2.7)$$

2.2 Gas Dynamics**Compressibility**

When considering the flow in one-dimension, the fluid properties in compressible flows are mainly affected by three factors: (i) the changes in the cross-sectional area, (ii) the friction, (iii) the heat transfer [Aksel and Eralp, 1994, pg. 79]. In the case at hand, factor (i) is mostly assumed to be negligible, i.e., the pipe cross-sectional area is considered constant.

Compressible flow in ANSYS Fluent Compressible flows are described by the standard continuity and momentum equations, and no extra treatment is needed, except the compressible treatment of density (see equation). The energy equation solved by Fluent incorporates the coupling between the flow velocity and the static temperature.

$$\rho = \frac{p_{op} + p}{\frac{R}{M_w} T} \quad (2.8)$$

Compressible flow problems might involve fluids that do not behave as an ideal gas. Such an example is flow under very high-pressure conditions which will not be correctly modeled using the ideal-gas assumption. Instead a real gas model need to be used.

Energy equations

$$\frac{\partial}{\partial t}(\rho E) + \nabla \cdot (\vec{v}(\rho E + p)) = \nabla \cdot \left(k_{eff} \nabla T - h \vec{J} + (\bar{\tau}_{eff} \cdot \vec{v}) \right) + S_h \quad (2.9)$$

In solid regions, the energy transport equation has the following form;

$$\frac{\partial}{\partial t}(\rho h) + \nabla \cdot (\vec{v} \rho h) = \nabla \cdot (k \nabla T) + S_h \quad (2.10)$$

The sensible enthalpy;

$$h = \int_{T_{ref}}^T c_p(T) dT \quad (2.11)$$

General theory of Gas Dynamics

For the verification cases a simplified form of flow is considered. Some assumptions that later will not hold, are made to generate a model, simple enough to solve as a classical gas dynamics problem. The three cases under consideration are; Fanno flow, Rayleigh flow and the combined Fanno-Rayleigh flow. The Fanno model considers adiabatic flow through a pipe, with only friction forces considered. The Rayleigh model on the other hand, considers pipe flow with heat transfer, where friction effects are negligible. The third setup is the simultaneous consideration of friction and heat transfer, and also the analytical model of highest relevance. All three model a pipe of constant cross-sectional area.

The Fanno and Rayleigh flow models are both quasi one-dimensional representations of steady-state flow. Both also make a joint set of assumptions on the fluid being a perfect gas (ideal and with constant heat capacity). Complete lists of the assumptions made in the two models can be found in Appendix 7.1.

In common for the three verification models are the following conservation equations, of mass and momentum;

$$\begin{aligned} \dot{m} &= \rho_1 A_1 V_1 = \rho_2 A_2 V_2 = \text{constant} \\ G &= \dot{m}/A = \rho_1 V_1 = \rho_2 V_2 = \rho V = \text{constant} \end{aligned} \quad (2.12)$$

$$(-F_f) + p_1 A_1 - p_2 A_2 = \rho_2 A_2 V_2^2 - \rho_1 A_1 V_1^2 \quad (2.13)$$

where the subtrahend F_f , the frictional force acting on the side walls, is not used for pure Rayleigh flow.

Equation of state, perfect gas

$$p = \rho RT \quad (2.14)$$

Second law of thermodynamics The thermodynamic relations

$$\begin{aligned} T ds &= dh - \frac{dp}{\rho} \\ T ds &= du - RT \frac{d\rho}{\rho} \end{aligned} \quad (2.15)$$

and the use of $dh = c_p dT$, $du = c_v dT$ and $p = \rho RT$, give us

$$ds = c_p \frac{dT}{T} - R \frac{dp}{p} = c_v \frac{dT}{T} - R \frac{d\rho}{\rho} \quad (2.16)$$

Fanno flow Except the three equations that the different flow models share, the following is specific for Fanno flow modelling.

First law of thermodynamics

$$h_{01} = h_1 + \frac{V_1^2}{2} = h_2 + \frac{V_2^2}{2} = h_{02} = h + \frac{V^2}{2} \quad (2.17)$$

$$\frac{d(M^2)}{M^2} = \frac{kM^2[1 + 0.5(k-1)M^2]}{1 - M^2} 4f \frac{dx}{D} \quad (2.18)$$

Rayleigh flow The specific equations for Rayleigh flow modelling are.

First law of thermodynamics

$$\dot{Q} = \dot{m}q = \dot{m}(h_{02} - h_{01}) = \dot{m} \left(h_2 + \frac{V_2^2}{2} - h_1 - \frac{V_1^2}{2} \right) \quad (2.19)$$

$$q = \int_a^b f(x) dx. \quad (2.20)$$

$$\frac{d(M^2)}{M^2} = \frac{k-1}{kRT} \frac{1+kM^2}{1-M^2} dq \quad (2.21)$$

Mixed flow

$$\frac{d(M)}{dx} = \frac{M \left(1 + \frac{\gamma-1}{2} M^2\right)}{1 - M^2} \left[\gamma M^2 \frac{f}{D} + \frac{1 + \gamma M^2}{2T_0} \frac{dT_0}{dx} - \gamma M^2 \frac{1}{A} \frac{dA}{dx} \right]$$

$$M(x=0) = M_1 \quad (2.22)$$

dT_0/dx can be determined from the energy equation, which can be expressed as:

$$q(\pi D) dx = \dot{m} c_p dT_0 \quad (2.23)$$

Pipe Hydraulics

In the field of hydraulics, we find a set of transformations, that come in handy. A complex pipe shape, can, by considering the friction added by diffusers, bends and turns, be converted to a equivalent straight pipe. The main equation for the theory of such conversions is;

$$\zeta_{tot} = \zeta_{loc} + \zeta_{friction} \quad (2.24)$$

where $\zeta = \lambda \cdot L/D$. The term ζ_{loc} accounts for the extra friction added by diffusers, bends or other geometrical obstacles to the flow.

Computational Fluid Dynamics

Finite volume method - FVM In the cases cited above, it is important that the conservation laws in their integral form are represented accurately. The most natural method to accomplish this is to discretize the integral form of the equations and not the differential form. This is the basis of a finite volume method. Further, in cases where strong conservation in integral form is not absolutely necessary, it is still physically appealing to use the basic laws in their most primitive form [Anderson Jr. et al., 2009, pg. 275].

The finite volume method (FVM) tries to combine the best from the finite element method (FEM), i.e., the geometric flexibility, with the best of the finite difference method (FDM), i.e., the flexibility in defining the discrete flow field (discrete values of dependent variables and their associated fluxes) [Anderson Jr. et al., 2009, pg. 278].

Representation of function values or fluxes better than piecewise constant or piece-wise linear is possible but rather complicated. Most FVM methods are only second-order accurate. For many engineering applications, this accuracy is sufficient. The development of finite volume methods with better accuracy is nowadays an area of very active research and there is still no clear insight in how to reach higher accuracy in an efficient way [Anderson Jr. et al., 2009, pg. 278].

Shocks form the most typical example of a discontinuous flow field. In case discontinuities occur, the solution of the partial differential equations is to be interpreted in a weak form, i.e., as a solution of the integral form of the equations. For example, the laws governing the flow through a shock, i.e., the Hugoniot-Rankine laws, are combinations of the conservation laws in integral form. For a correct representation of shocks, also in a numerical method, these laws have to be respected [Anderson Jr. et al., 2009, pg.275].

3

Methods

3.1 Method overview

A study of the processes occurring during the analysed discharges and their relative importance was performed. These comprised unsteady flow, compressible flow, diffusion, back pressure effect, cryogenic heat transfer and to a lesser extent frosting, air condensation. As a result of this study, the final model can be constructed to include the phenomena of high relevance.

The complexity of the problem geometry was simplified, in order to ease the computational cost. A set of simulations were actually run on a complex 3-dimensional model in ANSYS CFX, proving this approach to be too time-consuming. The geometry simplification is described in Section 3.4.

Data from tested cases of venting of helium are rare and/or hard to find [Weisend II, 2014]. Hence, the need for numerical simulations, in place of experimental results, as to investigate potential design options, is immense. An initial step of the project was focused on finding and choosing an appropriate software for modeling the flow. A numerical modeling software, ANSYS Fluent, to produce such simulations was chosen from some alternatives, according to requirements specified farther ahead, in Section 3.3.

The model was supplemented with case-specific scripts that take care of phenomena not handled by the main software program. For example the temperature- and time-dependent heat transfer coefficient was described by customized scripts, compiled to work with ANSYS Fluent. Also, all initial and boundary conditions were described by external scripts. The Fluent model constructed, as the main tool of this project, is henceforth denominated the Helium Vent Line model (HVL model). The HVL model was evaluated and modified accordingly in an iterative process, model parts were added and adjusted and the iterative procedure was repeated.

In order to evaluate the accuracy and parameter dependence of the HVL model, it was validated and benchmarked (verified). For *verification* three analytical cases from the field of gas dynamics were used; as described in the theory for gas dynamics, Section 2.2. For *validation*, the setup for the HVL was adjusted to simulate the equivalent of an experiment, with minimal changes in generic settings. The experiment for validation was chosen to be as close to the HVL thermodynamic circumstances as possible.

3.2 Problem description

Generic model

The model utilized and tuned for the different setups (validation case and HVL) were implemented in a similar way in ANSYS Fluent and rely on the same basic configurations. The three main procedures of CFD (computational fluid dynamics) are here treated, in sequential order; pre-processing, solving and post-processing; for the common settings of the different setups.

Validation case

The closest comparison case found for validation, [Chorowski et al., 2006], considers nitrogen gas vented in a copper pipe. This nitrogen experiment was constructed as to validate a numerical flow model of the venting of cryogenic helium at LHC. The fluid dynamical and thermodynamic state space was translated to the experiment's materials, dimensions and thermodynamic settings (the comparable state). The corresponding numerical model for this was presented in [Chorowski et al., 2004]. This model also served as a case for comparison with the HVL model.

Verification cases

The verification was carried out with simpler models for gas dynamics that were implemented in Matlab. The verification case was used twice; firstly as model for predicting the average flow profiles for the steady-state flow. This prediction also worked to approximate some initial settings for the HVL model. Secondly, as part of the post-processing, the verification model was tuned to the HVL results in order to reveal what settings of the semi-numerical verification model best mimics the more complex numerical HVL model. Thus, the same geometries are used as for the HVL.

The broad assumptions and limitations of the Fanno and Rayleigh models, see Appendix 7.1, lowered the expectations of perfect agreement with the final HVL, which treats the flow in a rather more sophisticated way, described in Sections 2.1, 2.2. However, these analytical/semi-numerical models worked

fine to help assess whether partial products of the HVL steady-state model were behaving according to theory.

To investigate the gas dynamics along the pipe, a Runge-Kutta (4) solver was employed, according to the method presented in [Bandyopadhyay and Majumdar, 2007]. This solver is implemented in Matlab; see scripts in Appendix 7.2.

HVL

Being validated and benchmarked the HVL is adjusted to the set of cases that are of interest at ESS. Some parameters are varied, to create a set of simulations, hopefully comprising a viable design option for ESS, and ultimately the optimal design option.

The standard pipe size used was (DN200), which was the size primarily considered due to the surroundings. A set of pressure drops were simulated. Finally, the models are run with both steady-state and transient configurations. Both were of interest when determining the possibility and sizing of a venting system.

Steady-state HVL Both steady-state and transient simulations are rendered for the HVL model. The steady-state simulations were less computationally expensive and rendered for a set of different pressure differences (1/8, 1/4, 1/2, 1, 2, 4 bar). These were simulated for two different heat transfer setups; for an idealized insulated pipe (no heat transfer to pipe from surroundings), and with convection added onto the outer surface of the pipe wall.

Transient HVL The transient simulations for the setup was much more computationally expensive, thus more time-consuming, and limited to one pressure difference setting (1/4 bar). The transient setup was also limited to the case with convection on the outer pipe walls, i.e., no transient simulation for an insulated pipe was carried out. It can be argued that the convection case would not differ dramatically from the insulated case, since the stored energy in the pipe will be the main source of heat in the initial phase, making the outer convection peripheral to the flow circumstances.

The transient flow was necessarily modeled in three stages. The first stage was a steady-state simulation of the initial condition for the whole pipe. This stage was simulated as a homogeneous pipe with a constant temperature wall at what will then be the inlet, and with outer pipe convection. The constant temperature used was calculated using a simple analytic thermal equilibrium

calculation, for conduction. This was done, since the initial temperature of the burst disk (i.e. the separating wall between the empty pipe and the internal fluid to be released) assumes a temperature influenced both by the pipe and the cooler structure containing the helium.

The second stage of the transient flow could be called *the initial pressure-wave propagation* and aims to simulate the immediate flow following the rupture of the inlet burst disk. This stage lasts until the pressure-wave reaches the the pipe outlet.

The third and last stage of the transient flow simulates what happens following stage two. The pipe continues to be filled with high density helium and the heat transfer influence on the flow increases. This stage was sensitive to wave reflections at the pipe outlet, which was also the main reason for the second and third stage to be simulated separately and a bit differently. The wave reflections, in the third stage, are avoided by a combination of model adjustments; the time-step is increased as not to capture minor wave reflections, and a viscous zone is introduced after the outlet to absorb reflections.

Argument for only doing with convection (not insulated case - short t-period and much energy stored in the wall, relate conduction coeff. with convection outside)

3.3 Choice of software

Alternatives A short investigation was made into the alternatives available for the project at hand. A set of three software choices were considered; firstly and secondly, commercial pieces of software from ANSYS, CFX and Fluent, and thirdly the freeware OPENFOAM. Early OPENFOAM was deselected, mainly because of the considerably higher amount of work demanded to model some of the phenomena of interest in that program. ANSYS was chosen before other commercial alternatives, due to license availability.

ANSYS The two software options provided by ANSYS, appeared highly appropriate for modeling all three setups. However, Fluent comprises most of the abilities in CFX, without lacking any of the more interesting advantages of CFX, see Foremost, sealing the deal for Fluent, was the good modeling apparatus for modeling 3D flow, as mapped to 2D (planar or axisymmetric). Fluent also has both pressure-based and density-based solver types, CFX lacks the latter. CFX was initially tested for some HVL simulations, but

early revealing the high number of computational nodes needed to resolve a long narrow pipe with thin wall. As discussed in [ANSYS CFX-Solver Theory Guide 2013], the density-based solver is preferable for compressible flows.

3.4 Pre-processing

Geometry simplification

To heavily decrease the geometry's computational complexity, the actual pipe geometry was converted with the help of pipe hydraulic theory, see Section 2.2, to a straight and simple pipe, at the expense of pipe elongation. Also, the complex configuration of venting mechanisms were disregarded in the simulations. Instead, these were replaced with one idealised rupture disk. The geometry after simplifications can be seen in Figure 3.1. Here, three sub-figures describe the same geometry. The top figures (1.a and 1.b) show the pipe after being simplified and elongated, and containing a fluid. The middle figures (2.a and 2.b) are the axis-symmetric projection of the circular pipe on a cylindrical wedge with the azimuth angle θ . This is the domain used by ANSYS Fluent for simulations, and the angle used is to $\alpha = 1^\circ$. Finally, the bottom figure shows the 2-dimensional representation of half of the pipe, which primarily is used during pre- and post-processing (e.g. setting of boundary conditions and interpreting results). On the right side the cross-sectional view of the circular pipe and the wedge can be seen.

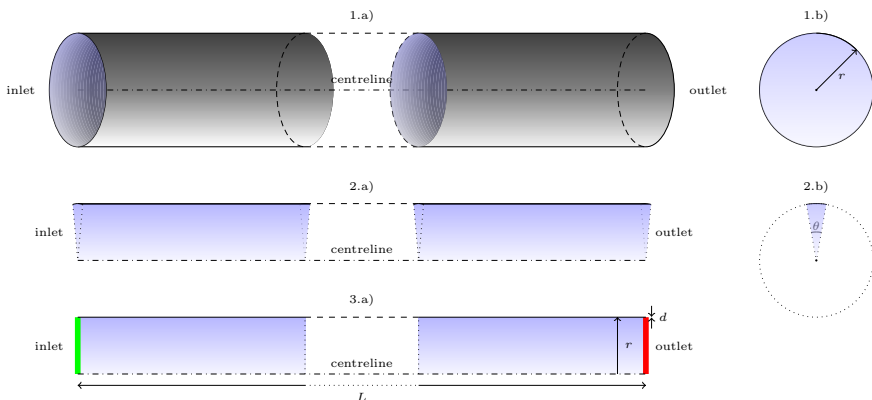


Figure 3.1 Simplified model geometry

Mesh

Several mesh configurations were tested and refined. The main candidates implemented are described shortly, and one of them can be viewed in Figure 3.4. In this 2D-view of the half cross-section of the initial part of the pipe, the refinement strategies are easily depicted. Both candidates implement *inflation* and *quad-dominant* element shape, for the fluid body, and a *tri-dominant* element shape for the solid body, i.e. the pipe wall.

The quad-elements are computationally preferable for fluid flow, and should optimally align with the flow direction. Inflation is a refinement strategy where the element size (perpendicular to the flow direction) is decreased gradually closer to the wall. This is a suitable, and often necessary, refinement in order to resolve the flow properties, that in a lot of aspects change drastically close to wall, in the boundary zone. (This is especially the case for the HVL since a *no-slip* boundary condition is used).

One of the mesh candidates furthermore implements a simple mesh refinement at the inlet, this serves mainly to resolve the almost explosive development of the initial wave front for the transient case. The mesh further away from the inlet is unchanged, and a similar but smaller mesh refinement zone is applied at the outlet, mainly to avoid minor backflows, and hence peripheral error messages when simulating.

The candidate not displayed in the figure, implements a strictly quad-elemental (fluid) mesh that is inflated at the wall, but uniform along the pipe, also lacking any refinement at the outlet. For the steady-state simulations, the flow properties are not predicted to have higher gradients at the inlet than in any other part of the pipe, and the optional refinement is only seen as a computational burden. In the transient case, however, it is considered in order to enable the computation of the drastic changes when the flow ensues. The drawback with this idea is when the high-gradient wave front of high resolution moves into a zone of larger elements.

The meshing strategy used is most easily described in Figure 3.4, where the mesh close to the inlet and outlet is displayed. The mesh in between the extremes can be assumed regular, with only minor deviations. The inlet and especially outlet areas are refined gradually in sections. A constant 'inflation' method is used in the adjacency of the wall, in order to capture the boundary zone behavior.

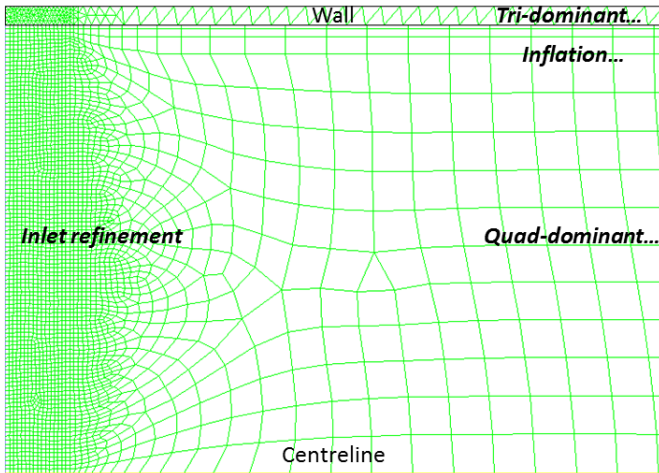
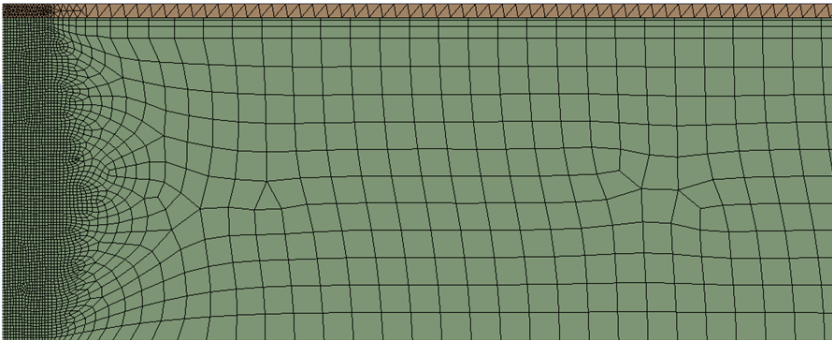


Figure 3.2 Pipe inlet mesh, displaying the main mesh refinement methods used.



Material settings

For material property implementation, two different sources were used, one implicit and the other explicitly implemented. Both fluids, helium and nitrogen, are available in ANSYS Fluent, as the "NIST real gas models". The NIST real gas models use the National Institute of Standards and Technology (NIST) Thermodynamic and Transport Properties of Refrigerants and Refrigerant Mixtures Database Version 7.0 (REFPROP v7.0). The REFPROP v7.0 database is dynamically loaded into the solver [*ANSYS FLUENT, User's Guide* 2009, pg. 487]. The equations employed by REFPROP v7.0 were pure-fluid equations based on the following three models; modified Benedict-Webb-Rubin (MBWR) equation of state, Helmholtz-energy equa-

tion of state, and extended corresponding states [ANSYS FLUENT, *User's Guide* 2009, pg. 488].

Boundary conditions and initialization

The boundary conditions were set by specifying 1D profiles or constants for representation of the fluid domain similar to part 3.a in 3.1. The profiles or constant could be made time- or property-dependent by writing scripts, so called user-defined functions (UDF).

Boundary conditions for steady-state simulations An iterative approach was applied for inlet turbulence parameters. The steady-state simulations were easily supported by the gas dynamics theory, introduced. A Runge-Kutta (4) solver was used to predict the pressure-driven flow's development corresponding to the setup's inlet and outlet pressures. From these results, the flow could be characterised. Approximate non-dimensional numbers were calculated. Using the flow parameters from gas dynamics, and using the formulas in [Anderson Jr. et al., 2009, pg. 264], the turbulence inlet parameters can be estimated and set at constant value across the inlet.

$$k_{inlet} = \frac{3}{2}(U_{inlet}I)^2 \quad (3.1)$$

$$5\% \leq I \leq 10\%$$

$$\omega_{inlet} = \frac{k^{1/2}}{C_{\mu}^{1/4}L} \quad (3.2)$$

These values were used for the first iteration for the steady-state solver. For later iterations, result values were used to specify a profile function for both values, that change in the radial direction. More specifically, a turbulence profile measurement was made at the current iteration, initially in the middle of the pipe. The profile measured was then used as turbulence profile at the inlet in the next iteration. As the profile approached the characteristics of a developed flow (see [Anderson Jr. et al., 2009, pg. 108]) the new measurements were made successively closer to the inlet. In order to comply with transient results, the model was also run for spatially constant turbulence inlet conditions.

BC and IC for transient simulations For the transient model, the boundary conditions were harder to specify. We were instead being content with a spatially constant value for the inlet boundary. The pressure and temperature were set according to the setup specification. Other parameters, primarily the turbulence parameters, were taken from the steady-state

model results. All inlet conditions, except temperature, were approximated to increase linearly from initial conditions (set uniformly in the entire pipe volume). Temperature was described by a smoother piece-wise linear function, since the solver seems highly sensitive to discontinuities in the temperature derivative.

3.5 Solver

Turbulence models chosen

Several models were used for turbulence. All models considered, were RANS (Reynolds-averaged Navier–Stokes) models. For most cases a $k-\omega$ model was used. However, $k-\epsilon$ models and the $k-k_t-\omega$ model were also tested for cases where deemed appropriate. Transient cases were treated almost exclusively with a $k-k_t-\omega$ model, since the flow characteristics ranged over a large set of flow types, chiefly when considering Re numbers.

3.6 Post-processing

Post-processing largely had to be handled in both the ANSYS software CFX-Post and Matlab. Most often data was averaged circumferentially within CFX-Post and exported to Matlab, where it could easily be co-plotted with other results (e.g., the Fanno and Rayleigh flow results).

4

Results

4.1 Benchmarking

The benchmarking results can be seen in Figures 4.1 and 4.2.

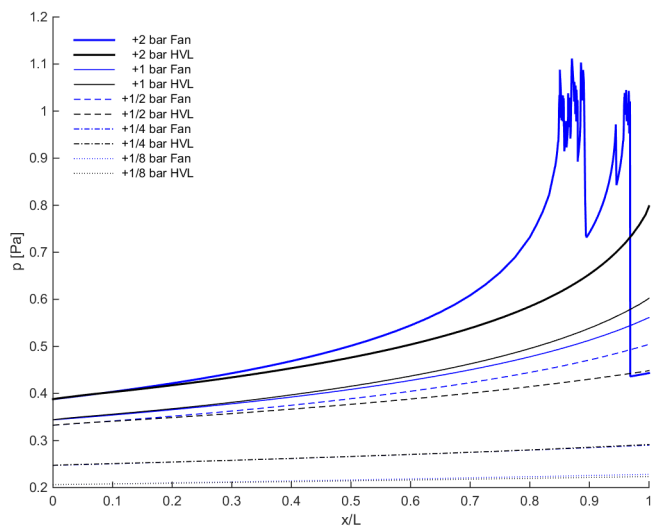


Figure 4.1 Benchmarking—Cross-sectional area average of Mach number along pipe. HVL steady-state simulation of insulated pipe compared with Fanno flow through RK4-method.

hello

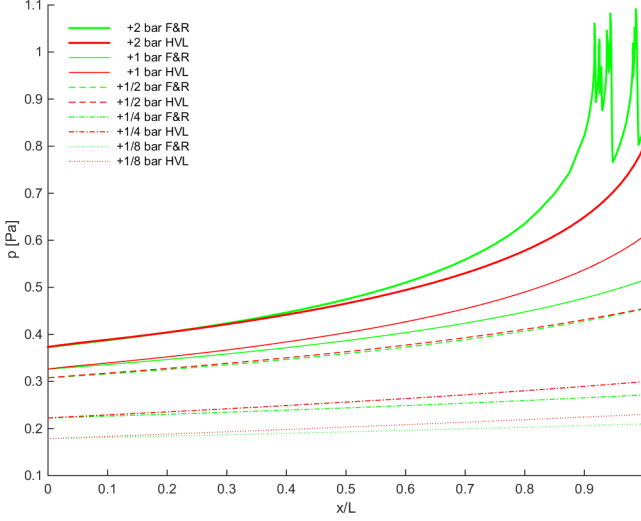


Figure 4.2 Benchmarking—Cross-sectional area average of *Mach number* along pipe. *HVL steady-state simulation with outer convection* compared with *mixed Fanno & Rayleigh flow* through RK4-method.

4.2 ESS CDL ventilation (HVL)

Steady-state results Pictures of averaged properties, comparison between insulated and convection cases, can be seen in Figures; 4.3, 4.4, 4.5, 4.6, 4.7 and 4.8.

The relations seen in Figures 4.2 and 4.2 were well approximated linearly. For insulated case:

$\dot{m}(p_0^+) = 15.26p_0^+ + 5.796$, with a norm of residuals 2.3% and maximal residual of 3.8%.

$Re(p_0^+) = 10^7 \cdot (4.062p_0^+ + 1.516)$, with a norm of residuals 2.7% and maximal residual of 4.0%.

For convection-exposed case:

$\dot{m}(p_0^+) = 15.18p_0^+ + 4.885$, with a norm of residuals 2.6% and maximal residual of 4.3%.

$Re(p_0^+) = 10^7 \cdot (4.028p_0^+ + 1.080)$, with a norm of residuals 2.9% and maximal residual of 4.0%.

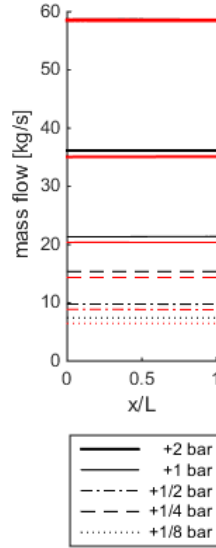


Figure 4.3 *Mass flow* for different setups of inlet-outlet pressure difference. Black, indicating insulated pipe and, red, pipe exposed to atmosphere (convection). The two lines coincide for the case with pressure difference $+4\text{bar}$.

Transient results The final setup results for the HVL case were presented. For visual clarity, the two simulation phases, described in Section 3.2, were plotted separately side by side.

Phase 1 - Pressure wave propagation Here the pressure wave propagating during the first 0.09 seconds after burst disk rupture. See Figures 4.11, 4.10, 4.12, 4.13, 4.14 and 4.15.

Phase 2 - Density wave propagation and pipe cool-down See Figures 4.11, 4.10, 4.12, 4.13, 4.14, 4.15, 4.16 and 4.17.

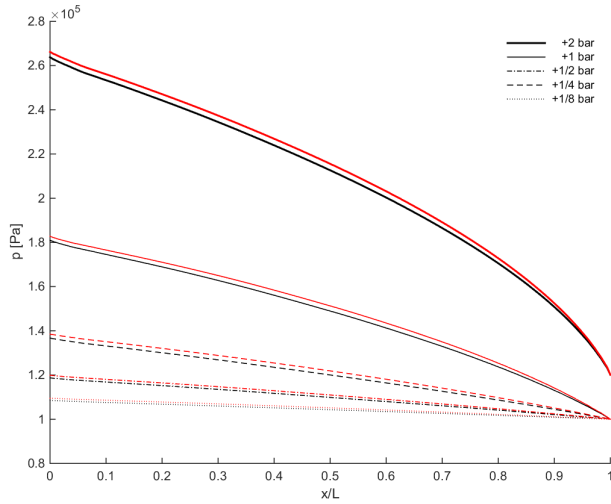


Figure 4.4 Cross-sectional area average of static *pressure* along pipe. Black, indicating insulated pipe and red, pipe exposed to atmosphere (convection), for different setups of inlet-outlet pressure difference.

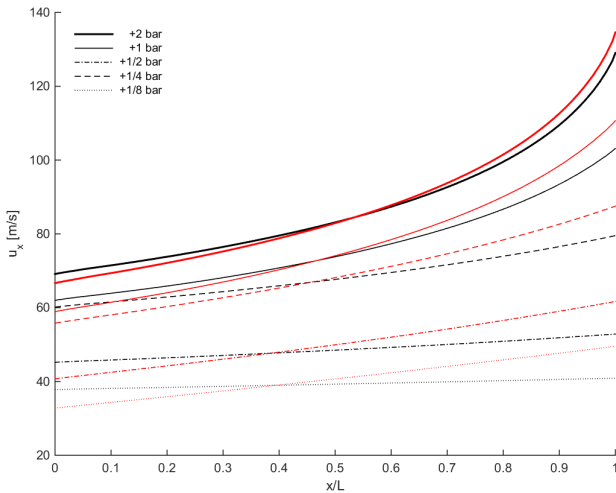


Figure 4.5 Cross-sectional area average of *axial velocity* along pipe. Black, indicating insulated pipe and red, pipe exposed to atmosphere (convection), for different setups of inlet-outlet pressure difference.

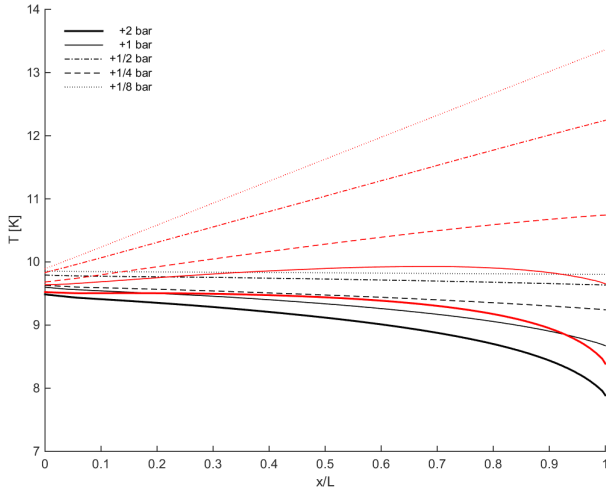


Figure 4.6 Cross-sectional mass flow average of *temperature* along pipe. Black, indicating insulated pipe and red, pipe exposed to atmosphere (convection), for different setups of inlet-outlet pressure difference.

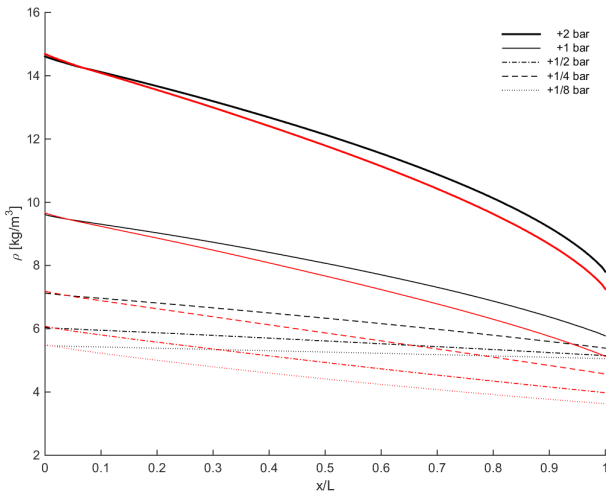


Figure 4.7 Cross-sectional area average of *density* along pipe. Black, indicating insulated pipe and red, pipe exposed to atmosphere (convection), for different setups of inlet-outlet pressure difference.

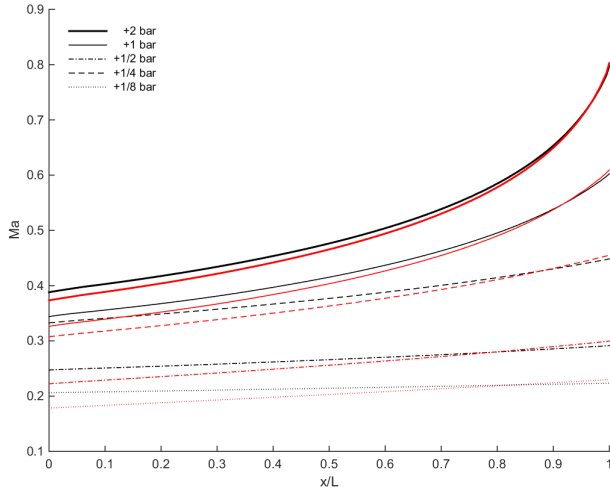
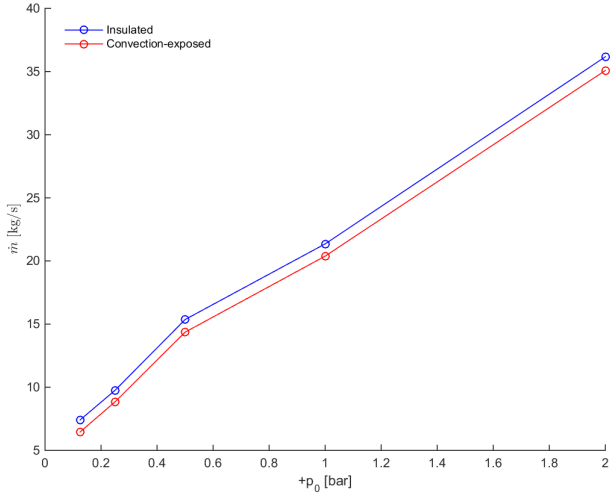
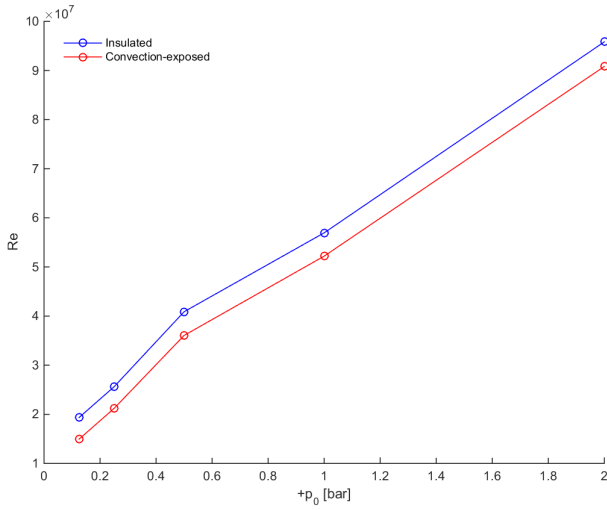


Figure 4.8 Cross-sectional area average of *Mach number* along pipe. Black, indicating insulated pipe and red, pipe exposed to atmosphere (convection), for different setups of inlet-outlet pressure difference.



(a) Massflow



(b) Reynolds number

Figure 4.9 Flow properties as function of the inlet-outlet total pressure difference.

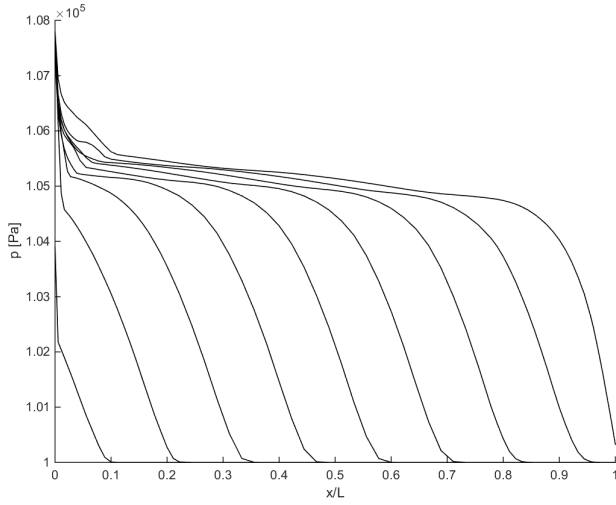
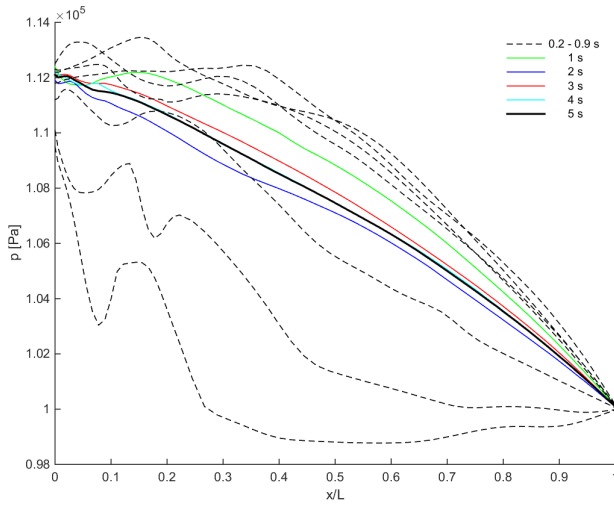
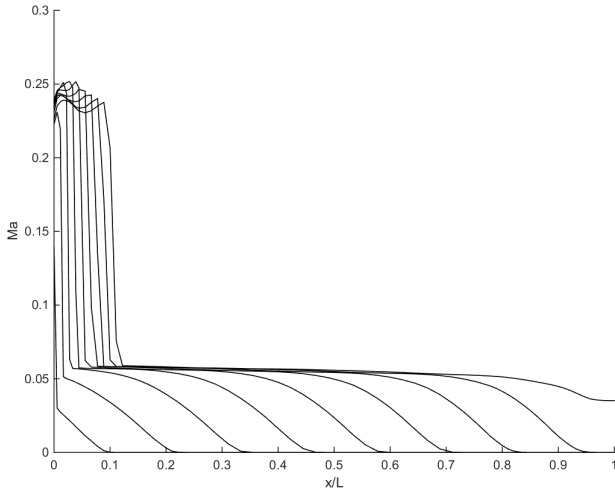
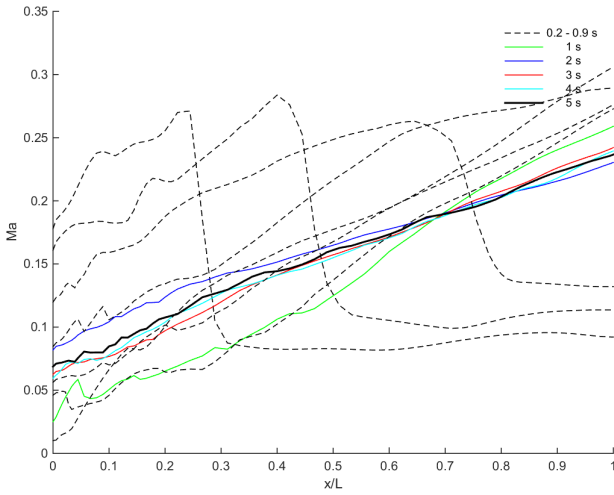
(a) Phase 1: $t = 0.01, 0.02, \dots, 0.09$ s(b) Phase 2: $t = 0.3, 0.4, \dots, 0.9$, s and 1, 2, ..., 5 s

Figure 4.10 Transient HVL—Cross-sectional area averaged *static pressure* along pipe.



(a) Phase 1: $t = 0.01, 0.02, \dots, 0.09$ s



(b) Phase 2: $t = 0.3, 0.4, \dots, 0.9$, s and 1, 2, ..., 5 s

Figure 4.11 Transient HVL—Cross-sectional area averaged *Mach number* along pipe.

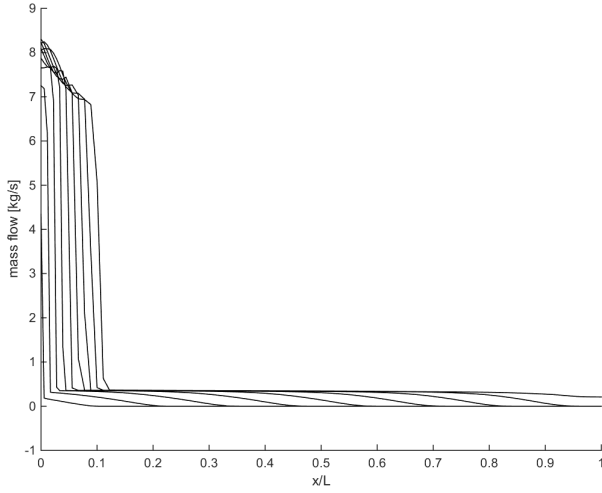
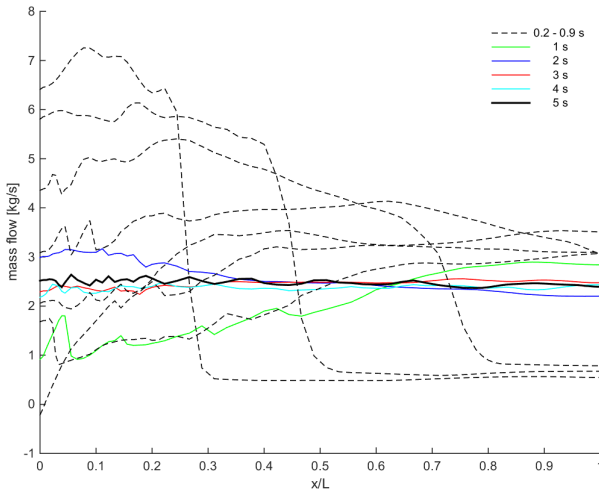
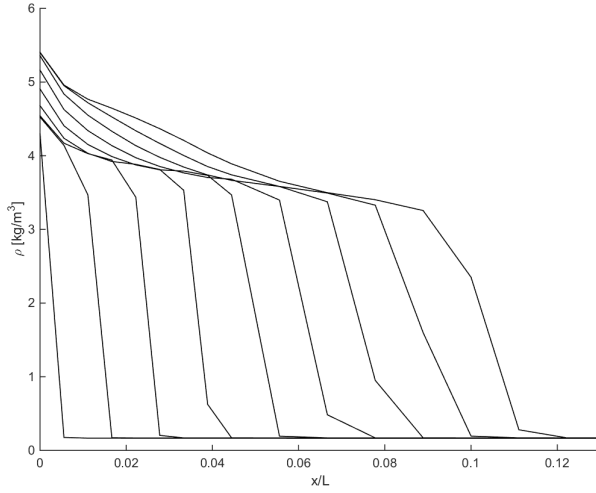
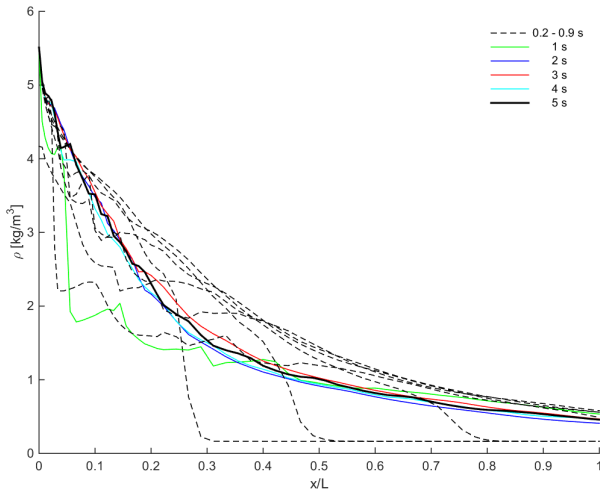
(a) Phase 1: $t = 0.01, 0.02, \dots, 0.09$ s(b) Phase 2: $t = 0.3, 0.4, \dots, 0.9$, s and 1, 2, ..., 5 s

Figure 4.12 Transient HVL—Cross-sectional area averaged *mass flow* along pipe.



(a) Phase 1: $t = 0.01, 0.02, \dots, 0.09$ s. Note x-axis scaling.



(b) Phase 2: $t = 0.3, 0.4, \dots, 0.9$, s and 1, 2, ..., 5 s

Figure 4.13 Transient HVL—Cross-sectional area averaged *density* along pipe.

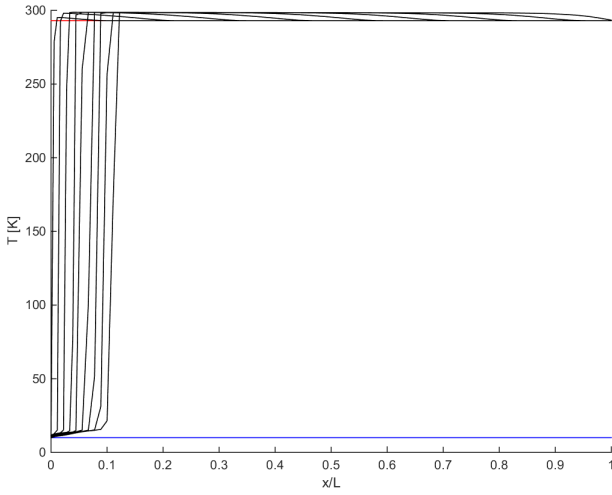
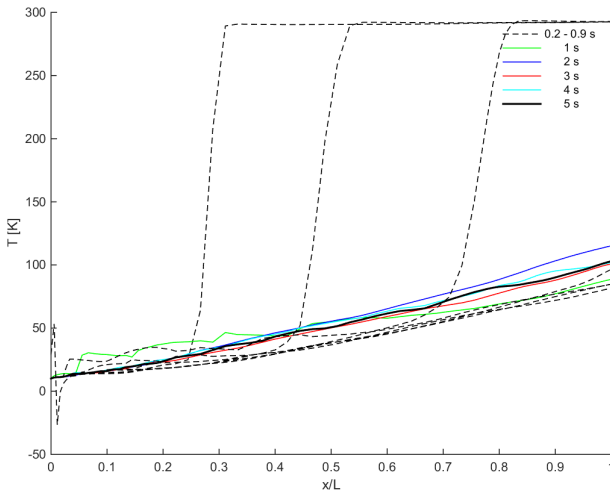
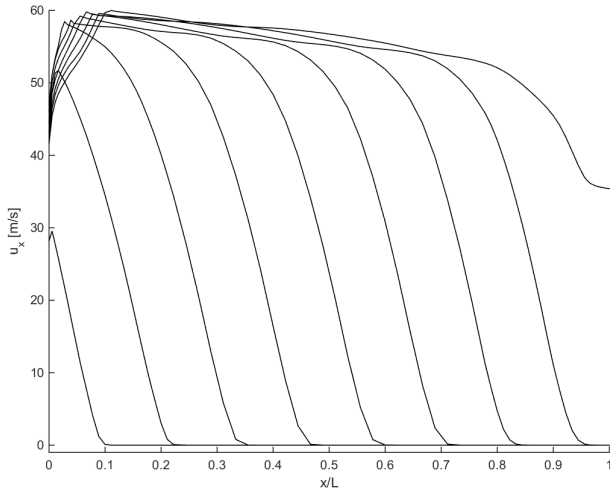
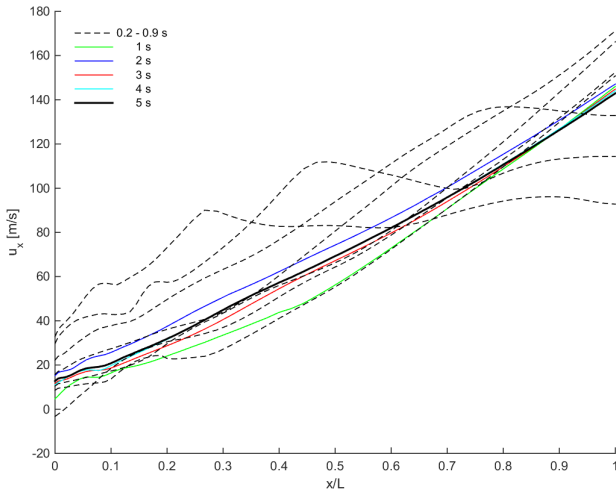
(a) Phase 1: $t = 0.01, 0.02, \dots, 0.09$ s(b) Phase 2: $t = 0.3, 0.4, \dots, 0.9$, s and 1, 2, ..., 5 s

Figure 4.14 Transient HVL—Cross-sectional mass flow averaged *static temperature* along pipe.

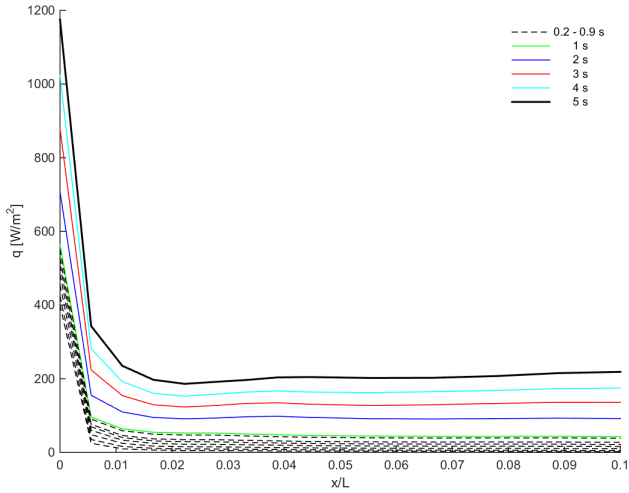


(a) Phase 1: $t = 0.01, 0.02, \dots, 0.09$ s

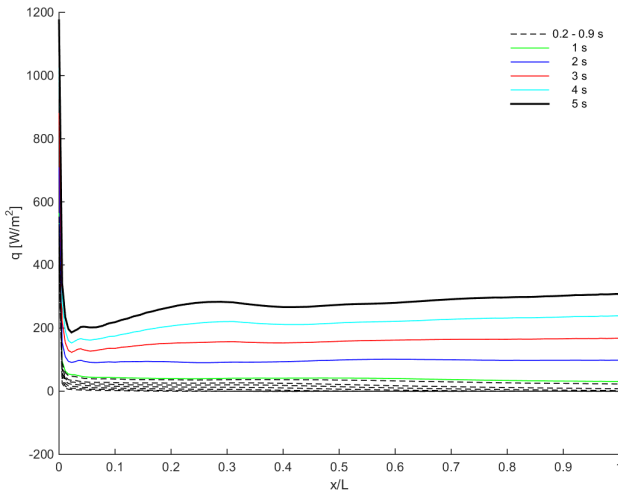


(b) Phase 2: $t = 0.3, 0.4, \dots, 0.9$, s and 1, 2, ..., 5 s

Figure 4.15 Transient HVL—Cross-sectional area averaged *axial velocity* along pipe.

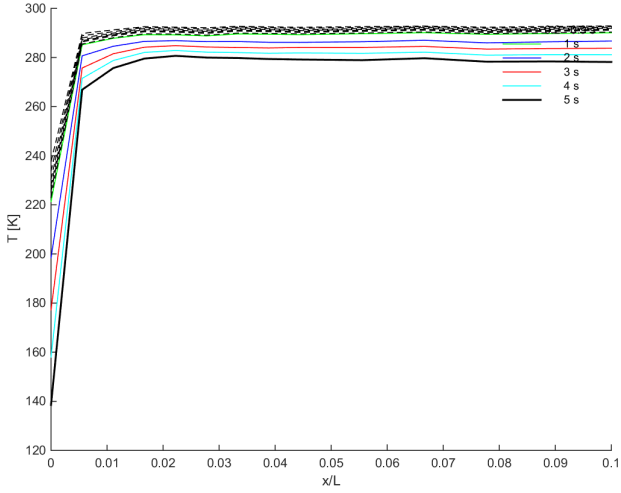


(a) For initial 10% of pipe, from inlet.

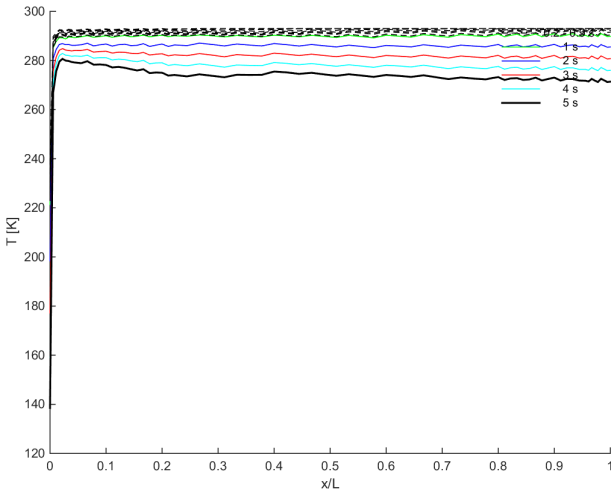


(b) Along entire pipe length.

Figure 4.16 Transient HVL phase 2—heat transfer; $t = 0.3, 0.4, \dots, 0.9, 1, 2, \dots, 5$ s; steel *heat transfer* along pipe wall.



(a) For initial 10% of pipe, from inlet.



(b) Along entire pipe length.

Figure 4.17 Transient HVL phase 2—wall temperature; $t = 0.3, 0.4, \dots, 0.9, 1, 2, \dots, 5$ s; steel temperature along pipe wall.

5

Discussion

Of all the physical processes involved in this kind of flow situation, only the processes of highest importance (compressibility, unsteady flow, shock wave propagation and heat transfer) were modeled. The complexity of the numerical CFD models made the processes of finding suitable configurations – for mesh, temporal discretization and property rendition – time-consuming. The simulation sensitivity to high gradients in property values, foremost pressure and temperature, made even simple cases highly computationally expensive.

A challenge for the numerical modeling was the comparably oblong geometry, and hence the long simulation time for the shock wave to travel the entire pipe length. The sharp shock wave front demanded high resolution in mesh at the location of the shock wave front at every time frame. A static mesh, either leads to a divergent simulation, or requires high resolution along the entirety of the pipe length. An alternative, dynamic meshing exists, but was never employed.

The use of ANSYS Fluent for a compressible flow of a fluid modeled with a real gas model, is extremely time-consuming. A lot of details that might not be relevant to the query at hand require attention that is out of proportion. If the most critical parameters of interest had been stated more clearly a priori some of this time consuming attention might have been avoided.

At the start of this thesis no comparable flow experiments existed to help guide the sizing of the venting pipe. While not comprising any empirical testing, this thesis aimed to create a numerical simulation close enough to a realistic course of events for the venting of cold helium. As such, the results form a basis for further investigation, and highlights some of the modeling pitfalls that preferably should be avoided.

6

Conclusion

The results of the transient simulations in ANSYS Fluent (HVL) and the steady-state ones, are preferably regarded as simulations of two different heat transfer phases. The transient case simulates the heat transfer situation, starting with a warm pipe containing warm helium and the subsequent replacement of helium and cooling of the pipe wall. The transient simulation would have to be run for longer than the simulated 5 s, as to have it reach the steady-state solution. Comparing the final transient static temperature curve in Figure 4.2 with the equivalent steady-state curve, also reveals the premature final step of the transient simulation. Together the steady-state and transient simulations paints a more complete picture of what a venting process would look like.

The almost linear relation between the non-dimensional flow properties and the stagnation pressure is helpful for future estimations. Also the comparison between the Fanno & Rayleigh models and the simulations contributes with a sense of for which pressure differences the much less expensive semi-numerical method could come in handy.

6.1 Recommendations / Future work

In the ANSYS software, there exist fundamentally different approaches to meshing, one of which might render the transient simulations more manageable. This approach uses a *dynamic mesh* that, as the name suggests, changes with time, adjusted for some relevant parameter, e.g., a property gradient, when needed. A dynamic mesh introduces the computation of new mesh configurations, and hitherto requires more memory, but hopefully fewer iterations every time-step.

7

Appendices

7.1 Appendix - Model assumptions

Fanno and Rayleigh flow

Shared assumptions

- i. Quasi-1D flow; constant flow profile (all properties; velocity, density etc.)
- ii. Perfect gas (ideal gas and constant c_p)
- iii. Steady-state flow (not applicable on transient flow)
- iv. Cross-sectional area constant along pipe, $dA(x) = 0, \forall x$.
- v. Constant viscosity, Hepak value based on average thermodynamic state.
- vi. $M_{outlet} \leq 1$

Fanno flow assumptions

- vii. Adiabatic system; no heat transfer to system, $\dot{Q} = 0$.
- viii. Only friction, proportional to $f \cdot L/D$, where $f = moody(Re, \epsilon)$.

Rayleigh flow assumptions

- vii. Non-adiabatic system; constant heat transfer along pipe.
- viii. No external (pipe-to-fluid) friction considered.

Numerical model—HVL (ANSYS Fluent)

- i. 2D model
- ii. Multiple choice; eg. Refrop NIST real gas model.
- iii. Steady-state and transient flow modelling capabilities.
- iv. Cross-sectional area

7.2 Appendix 3 - Code

Matlab code

Fanno and Rayleigh scripts Here, are the scripts that implemented the Runge-Kutta 4 solver for the Fanno, Rayleigh and mixed flow differential equations from gas dynamics.

Listing 7.1 rayleighflowfn.m – Differential equation, Rayleigh flow

```
function dM_dx = rayleighflowfn(x,M)
gamma = 5/3;

D = 0.1094;
T0 = 20;
q = 1700; % W/m2
mdot = 5;
cp = 5200;
dM_dx =
    ((M*(1+0.5*(gamma-1)*M^2))/(1-M^2))*(1+gamma*M^2)*q*pi*D/(2*T0*mdot*cp);
return
```

Listing 7.2 fannoflowfn.m – Differential equation, Fanno flow

```
function dM_dx = fannoflowfn(x,M)
gamma = 5/3;
D = 2*0.106771;
A = pi*(D/2)^2
epsilon = 1.5e-5;
ed = epsilon/D;

mflowrate = 30.1641; % the same at outlet
rho_v = mflowrate/A;
mu_ave_volave = 2.0767201e-06;

Re = rho_v*D/mu_ave_volave;
f = moody(ed,Re);
```

```

%T0 = 20;
%q = 10; % W/m2
%mdot = 5;
%cp = 5190;
% TIMES (1/2) to get same solution as Matlab fn
dM_dx = (1/2)*(M*(1+0.5*(gamma-1)*M^2))/(1-M^2)*(gamma*M^2*f/D); %+
        (1+gamma*M^2)*q*pi*D/(2*T0*mdot*cp));
return

```

Listing 7.3 flowfn.m – Differential equation, mixed flow

```

function dM_dx = flowfn(x,M)
gamma = 5/3;
D = 0.1094;
epsilon = 1.5e-5;
ed = epsilon/D;

rho = 0.9572; % take average
v = 279.44; %
mu = 9.768e-6;
Re = rho*v*D/mu;
f = moody(ed,Re);

T0 = 20;
q = 3000; % W/m2
mdot = 5;
cp = 5200;
dM_dx = (M*(1+0.5*(gamma-1)*M^2))/(1-M^2)*(gamma*M^2*f/D +
        (1+gamma*M^2)*q*pi*D/(2*T0*mdot*cp));
return

```

Listing 7.4 Runge-Kutta4 solver

```

%% USE Matlab "flowfanno" to get inlet Mach nbr (only when outlet
    Mach=1)
clear all
close all

gamma = 5/3;
L = 10;
D = 2*0.106771;
epsilon = 1.5e-5;
A = pi*(D/2)^2

% Inlet conditions

```

```
mflowrate = 30.1641; % the same at outlet
rho_v = mflowrate/A;

% estimated mu
mu_ave_volave = 2.0767201e-06; %molecular viscosity from Fluent -
    volume average
mu_ave_massave = 2.0807656e-06; %molecular viscosity from Fluent -
    mass average

Re = rho_v*D/mu_ave_volave;
ed = epsilon/D;
ff = moody(ed,Re);
fanno = ff*L/D;

% Calculate M1
[mach_f1, T_f1, P_f1, rho_f1, velocity_f1, PO_f1, fannol] =
    flowfanno(gamma,fanno,'fannosub');

% Runge-Kutta4 solver for the mixed Fanno and Rayleigh flow
% Renders solution along x-axis

M1 = mach_f1 % Highest M1= 0.3544 for L=10 for MIXED flow
    % Highest M1= 0.3577 for L=10 for Fanno flow
    % Highest M1= 0.84 for L=10 for Rayleigh flow

% Assigned values
xspan = [0,10];

%%%% MIXED flow %%%%
% [T,Y] = solver(odefun,tspan,y0);
%[x,M] = ode45(@flowfn,xspan,M1);
%plot(x,M)

%%%% FANNO flow %%%%
[xFa,MFa] = ode45(@fannoflowfn_GOALCASE1,xspan,M1);
hold on
plot(xFa,MFa,'r')
outletMFa = MFa(end)
inletMFa = MFa(1)

%%%% RAYLEIGH flow %%%%
%[xRa,MRa] = ode45(@rayleighflowfn,xspan,M1);
%plot(xRa,MRa,'g')
```

Bibliography

- Aksel, M. H. and O. C. Eralp (1994). *Gas Dynamics*. Prentice Hall International, Hertfordshire, UK.
- Anderson Jr., J. D., J. Degroote, G. Degrez, E. Dick, R. Grundmann, and J. Vierendeels (2009). *Computational Fluid Dynamics - An Introduction*. Ed. by J. Wendt. Springer-Verlag Berlin Heidelberg, Berlin, Heidelberg, Germany.
- ANSYS CFX-Solver Theory Guide* (2013). Release 15.0. ANSYS Inc. Canonsburg, Pennsylvania, USA.
- ANSYS FLUENT, User's Guide* (2009). Release 12.0. ANSYS Inc. Canonsburg, Pennsylvania, USA. URL: https://www.afs.enea.it/project/neptunius/docs/fluent/html/ug/main_pre.htm.
- Bandyopadhyay, A. and A. Majumdar (2007). “Modeling of Compressible Flow with Friction and Heat Transfer Using the Generalized Fluid System Simulation Program (GFSSP)”. In: *Thermal Fluid Analysis Workshop (TFAWS)*. Cleveland, Ohio, USA.
- Chorowski, M., J. Fydrych, and G. Riddone (2004). *Flow and Thermo-mechanical Analysis of the LHC Sector Helium Relief System*. Tech. rep. 780. LHC Project Report. CERN & Wrocław University of Technology, Geneva, Switzerland & Wrocław, Poland.
- Chorowski, M., J. Fydrych, and G. Riddone (2006). *Experimental Validation of the LHC Helium Relief System Flow Modeling*. Tech. rep. 859. LHC Project Report. CERN & Wrocław University of Technology, Geneva, Switzerland & Wrocław, Poland.
- Eriksson, R., (Ed.) (2008). *European Spallation Source The Unique Capabilities of ESS*. URL: <https://europeanspallationsource.se/unique-capabilities-ess>.
- Fydrych, J. (15, 2014). Personal communication.

Bibliography

- Pipework components — Definition and selection of DN (nominal size)* (1995). Standard. ISO 6708:1995. International Organization for Standardization, Geneva, Switzerland.
- Pipe components — Definition of nominal pressure* (1983). Standard. ISO 7268:1983. International Organization for Standardization, Geneva, Switzerland.
- Peggs, S. and R. K. (Ed.) (2013). *ESS Technical Design Report*. Tech. rep. ESS-doc-274-v15. European Spallation Source, Lund, Sweden.
- Weisend II, J., C. Darve, S. Gallimore, W. Hees, J. Jurns, T. Köttig, P. Ladd, S. Molloy, T. Parker, and X. Wang (2014). “Status of the ESS Cryogenic System”. In: *AIP Conference Proceedings*. Vol. 1573. European Spallation Source. Lund, Sweden, pp. 633–638.
- Weisend II, J. (4, 2014). Personal communication.

Lund University Department of Automatic Control Box 118 SE-221 00 Lund Sweden		<i>Document name</i> MASTER'S THESIS	
		<i>Date of issue</i> October 2020	
		<i>Document Number</i> TFRT-6117	
<i>Author(s)</i> Jonathan Persson		<i>Supervisor</i> John Weisend II, ESS, Sweden Jaroslav Fydrych, ESS, Sweden Johan Revstedt, Dept. of Energy Sciences, Lund University, Sweden Rolf Johansson, Dept. of Automatic Control, Lund University, Sweden Bo Bernhardsson, Dept. of Automatic Control, Lund University, Sweden (examiner)	
<i>Title and subtitle</i> Numerical modelling of cold helium safety discharges from the cryogenic distribution line			
<i>Abstract</i> <p>The European Spallation Source, ESS, is a project currently with 17 Partner Countries, and with Sweden and Denmark as host nations. The ESS main facility is being constructed in Lund, to ultimately become the world's most powerful neutron source, providing around 30 times brighter neutron beams than any earlier facility.</p> <p>The Linear Accelerator, Linac, at the heart of ESS is fundamentally powered by superconducting cavities that require extremely low temperatures to operate, namely 2K (-271 °C). The cooling/cryogenic fluid, helium, is supplied to the cavities through a complex cryogenic distribution system (CDS). At abnormal failure modes, to protect against unwanted over-pressurisation, this system needs to be vented through pressure safety valves. To avoid helium discharges into the tunnel the safety valves will discharge cold helium into a vent line, which transfer the helium into the external environment. Usually the most critical failure mode is a loss of insulation vacuum, which exposes the CDS to a sudden rise of heat loads.</p> <p>This thesis investigates the most critical phenomena for the non-insulated vent line flows. Due to a lack of simple engineering descriptions of these unsteady flows, a set of complex numerical models will support a proper vent line sizing proposal. A commercial numerical software, ANSYS Fluent, is used and compared with simpler solution methods for differential equations derived from Fanno and Rayleigh flow theories.</p>			
<i>Keywords</i>			
<i>Classification system and/or index terms (if any)</i>			
<i>Supplementary bibliographical information</i>			
<i>ISSN and key title</i> 0280-5316			<i>ISBN</i>
<i>Language</i> English	<i>Number of pages</i> 1-50	<i>Recipient's notes</i>	
<i>Security classification</i>			